

Published in final edited form as:

Sci Immunol. 2022 March 04; 7(69): eabg5539. doi:10.1126/sciimmunol.abg5539.

Single-cell transcriptional profiling informs efficient reprogramming of human somatic cells to cross-presenting dendritic cells

Fábio F. Rosa^{1,2,3,4}, Cristiana F. Pires^{1,2,3}, Ilya Kurochkin^{1,2,5}, Evelyn Halitzki^{1,2}, Tasnim Zahan^{1,2}, Nejc Arh^{1,2}, Olga Zimmermannová^{1,2}, Alexandra G. Ferreira^{1,2,3,4}, Hongzhe Li⁶, Stefan Karlsson¹, Stefan Scheding^{6,7}, Carlos-Filipe Pereira^{1,2,3,*}

¹Molecular Medicine and Gene Therapy, Lund Stem Cell Centre, Lund University, BMC A12, 221 84 Lund, Sweden

²Wallenberg Centre for Molecular Medicine, Lund University, BMC A12, 221 84 Lund, Sweden

³Centre for Neuroscience and Cell Biology, University of Coimbra, Largo Marquês do Pombal 3004-517 Coimbra, Portugal

⁴Doctoral Programme in Experimental Biology and Biomedicine, University of Coimbra, Coimbra, Portugal

⁵Skolkovo Institute of Science and Technology, Nobel Street, Building 3, Moscow 143026, Russia

⁶Division of Molecular Hematology, Department of Laboratory Medicine, Lund University, BMC B12, 221 84 Lund, Sweden

⁷Department of Hematology, Skåne University Hospital Lund, Skåne, 222 42 Sweden

Abstract

Type-1 conventional dendritic cells (cDC1s) are rare immune cells critical for the induction of antigen-specific cytotoxic CD8⁺ T-cells. The genetic program driving human cDC1 specification remains largely unexplored. We have previously identified PU.1, IRF8 and BATF3 transcription factors as sufficient to induce cDC1 fate in mouse fibroblasts but reprogramming of human somatic cells was limited by low efficiencies. Here, we investigated single-cell transcriptional dynamics during human cDC1 reprogramming. Human induced cDC1s (hiDCs) generated from embryonic fibroblasts gradually acquire a global cDC1 transcriptional profile and activate antigen presentation signatures. Importantly, other DC subsets are not induced at the single-cell level. We extracted gene modules associated with successful reprogramming and identified inflammatory signaling and the cDC1-inducing transcription factor network as key drivers of the process.

Combining IFN-γ, IFN-β and IFN-α with constitutive expression of cDC1-inducing transcription

*Corresponding author: filipe.pereira@med.lu.se.

Author contributions: F.F.R., C.F.P., T.Z., N.A., O.Z. and A.G.F. conducted reprogramming experiments and analyzed the data; H.L. and S.S. performed bone marrow aspirations and MSC generation. S.K. contributed with lentiviral vectors; F.F.R., I.K. and E.H. analyzed scRNA-seq and ChIP-seq datasets; F.F.R., C.F.P. and C-F.P. designed the experiments and wrote the manuscript.

Competing interests: F.F.R., C.F.P. and C-F.P. have equity interest in Asgard Therapeutics AB, which develops cancer immunotherapies based in DC reprogramming technologies. F.F.R., C.F.P. and C-F.P. are inventors of PCT/IB2018/052378 and priority application filed on 2021-05-19 by Asgard Therapeutics protecting the intellectual property described here.

factors lead to improvement of reprogramming efficiency by 190-fold. hiDCs uptake dead cells, secrete inflammatory cytokines and perform antigen cross-presentation, a key cDC1 function. This approach allowed efficient hiDC1 generation from adult fibroblasts and mesenchymal stromal cells. Mechanistically, PU.1 shows dominant and independent chromatin targeting at early phases of reprogramming, recruiting IRF8 and BATF3 to shared binding sites. The cooperative binding at open enhancers and promoters leads to silencing of fibroblast genes and activation of a cDC1 program. These findings provide mechanistic insights into human cDC1 specification and reprogramming and represent a platform for generating patient-tailored cDC1s, a long-sought DC subset for vaccination strategies in cancer immunotherapy.

Introduction

Dendritic cells (DCs) orchestrate innate and adaptive immune responses. Classically, human DCs are divided in 4 main subsets: conventional type 1 (cDC1s) and type 2 (cDC2s), plasmacytoid (pDCs), and monocyte-derived dendritic cells (moDCs), each defined by specific transcriptional regulators, surface markers and functional properties (1). The cDC1 subset, evolutionary conserved across mammalian species, is controlled by a network of transcription factors, including PU.1, IRF8 and BATF3 (2, 3). In mice, PU.1 promotes chromatin remodelling at the *Irf8* locus required to initiate expression and drive cDC1 differentiation from progenitors (4). High levels of IRF8 are then required throughout cDC1 specification and maintained by an auto-activation loop that becomes BATF3-dependent during the pre-cDC1 to cDC1 transition (5, 6). The inter-dependency of these transcriptional regulators and the mechanisms underlying chromatin engagement at the onset of human cDC1 specification remains largely unexplored.

Recent studies have revealed the heterogeneous nature of human DCs and identified new DC sub-populations with single-cell RNA sequencing (scRNA-seq) (7). Human cDC1s are characterized by surface expression of CD141, CADM1, CLEC9A and XCR1 (1), secrete immune-modulatory cytokines, including IL-12, interferons (IFNs) and CXCL10, and perform antigen cross-presentation to CD8⁺ T-cells, critical processes for inducing anti-tumor immune responses (8, 9). Accordingly, cDC1 abundance in human tumors was associated with patient survival and responsiveness to checkpoint inhibitors (9, 10). However, human cDC1s are very rare *in vivo*, so their study and use for cancer immunotherapy require methods to generate functional cDC1s *in vitro*. Human CD34⁺ bone marrow (BM) progenitors were used to derive CD141⁺ cDC1s *in vitro* in the presence of FLT3L, SCF, GM-CSF and IL-4 (8). More recently, FLT3L was combined with Notch signalling to favour cDC1 differentiation (11, 12). The generation of cDC1-, cDC2- and pDC-like cells from induced pluripotent stem cell (iPSC) cultures was also demonstrated (13). However, these protocols are complex, require feeder layers and generate multiple DC subsets with conflicting functions. Thus, new strategies to generate homogeneous populations of human cDC1s *in vitro* are warranted (14).

Direct reprogramming offers a novel strategy to generate cells for regenerative medicine and immunotherapy (15). Reprogramming of fibroblasts into various cell types including macrophages, neurons and cardiomyocytes was achieved without transiting through

pluripotency (16). We have recently shown that the transcription factors PU.1, IRF8 and BATF3 (PIB) are sufficient to convert mouse embryonic fibroblasts (MEFs) into cDC1-like cells (17). MEF-derived induced DCs (iDCs) acquire cDC1 phenotype, transcriptional program and functionality, including the ability to cross-present antigens to CD8⁺ T-cells. Moreover, we showed that overexpression of PIB in human fibroblasts yielded a small population of cDC1-like cells, highlighting the need to understand the principles governing DC reprogramming and optimize its efficiency in human cells. The heterogeneity and asynchronicity of direct reprogramming make it difficult to uncover fundamental mechanisms using population-based analysis. Several reports have described the utility of scRNA-seq to identify intermediate populations that emerge during reprogramming (18, 19), map clonal dynamics (20), and dissect successful and unsuccessful trajectories (19), leading to strategies for increased reprogramming efficiency (18, 20, 21). Given the emerging potential of scRNA-seq to uncover DC heterogeneity and the biology of direct reprogramming, we asked whether this approach could be used to inform and improve human DC reprogramming.

Results

Transcriptional profiling of human DC reprogramming at the single cell level

To induce DC fate in Human Embryonic Fibroblasts (HEFs), we used a polycistronic construct encoding PU.1, IRF8 and BATF3 separated by 2A sequences (PIB), cloned in a Doxycycline (Dox)-inducible lentiviral vector (TetO-PIB) (17) (Fig. 1A). After transducing HEFs with PIB, we observed the emergence of a CD45⁺ cell population at day 3 and a small population of CD45⁺HLA-DR⁺ cells from day 6 to day 9 with DC-like morphology (Fig. 1B-D) that we named human induced DCs (hiDCs). To elucidate transcriptional changes, we performed scRNA-seq using the 10X Chromium system. 45,870 cells were profiled from 3 donors, including peripheral blood cDC1s, cDC2s, pDCs, non-transduced HEFs (d0), hiDCs at day 3 (CD45⁺, d3), day 6 (CD45⁺, d6) and day 9 (CD45⁺HLA-DR⁻, d9 DR⁻; CD45⁺HLA-DR⁺, d9 DR⁺) (Fig. 1E, fig. S1, fig. S2A, table S1). t-Distributed stochastic neighbor embedding (t-SNE) visualization highlighted four clusters: HEFs (*ACTA2*⁺), cDC1s (*CLEC9A*⁺), cDC2s (*CD1C*⁺) and pDCs (*IL3RA*⁺) (Fig. 1E, fig. S2B, table S2). Genes encoding CD45 (*PTPRC*) and HLA-DR (*HLA-DRA*) used to purify hiDCs were not detected in HEFs (fig. S2B). While hiDC d3 and d6 did not map specifically to any clusters, hiDCs d9 mapped with cDC1s, with DR⁺ being closer to cDC1s than DR⁻ (Fig. 1E, fig S2A). These data suggest human cDC1 reprogramming requires a timeframe of 9 days and the CD45⁺HLA-DR⁻ represent a partial reprogrammed cell state. Accordingly, genes upregulated at later stages of reprogramming showed enrichment in immune pathways and ontologies, suggesting the progressive acquisition of a cDC1 transcriptional program (fig. S2C). Next, we integrated our single cell data with a publicly available DC dataset (7) using scPred (22). As expected, we observed that 53.8% of purified cDC1s were assigned to the DC1 subset, 66.9% and 29.8% of cDC2s to the DC2 and DC3 subsets, respectively, and 66.5% of pDCs to the DC6 subset (fig. S3). While HEFs were unaffiliated, 1.3% of d3, 5.3% of d6, 14.4% of d9 DR⁻ and 36.7% of d9 DR⁺ hiDCs were assigned specifically to the DC1 subset, suggesting that PU.1, IRF8 and BATF3 progressively impose a cDC1-like transcriptional program in HEFs with a degree of heterogeneity that does not

cross subset boundaries (Fig. 1F-G). DC1-affiliated cells express higher levels of the cDC1-specific genes *CADM1* and *WDFY4* when compared to their unaffiliated counterparts (7) (Fig. 1H). Accordingly, hiDCs expressed the cDC1 surface markers CD141 ($30.1\pm14.9\%$), CD38 ($34.2\pm12.9\%$) and CLEC9A ($10.6\pm1.7\%$) (fig. S4A-C). cDC2 (CD1C and CD11b) or pDC (CD123) markers were not detected (fig. S4B) (7). CD135/FLT3 receptor and the myeloid marker CD33 were detected at low levels. As expected, expression of T-cell (CD3), macrophage (CD14), granulocyte (CD15), B cell (CD19) and NK cell (CD56) markers was not detected (fig. S4D). Next, we extracted the most variable genes across the dataset and grouped them in 5 clusters (Fig. 1I). Cluster 1 contains genes highly expressed in HEFs and silenced during reprogramming. Cluster 2 highlights early transcriptional changes during reprogramming and cluster 3 includes the cDC1-specific genes *C1orf54*, *ANPEP*, *TACSTD2* and *SLAMF8* (7, 23, 24) highly expressed in d9 hiDCs and cDC1s (Fig. 1J). Cluster 4 and cluster 5 contain genes highly expressed in cDC2s and pDCs, respectively. Interestingly, d9 hiDCs express high levels of antigen processing and cross-presentation genes including *PSMB9*, *TAPI* and *HLA-C* (Fig. 1K-M). Indeed, surface expression of the co-stimulatory molecules CD40, CD80 and CD86 was detected in hiDCs, $33.6\pm14.3\%$, $30.7\pm1.1\%$, and $16.5\pm3.5\%$, respectively (fig S4E-F), suggesting that reprogrammed cells have acquired T-cell stimulatory capacity. Together, these data show that PIB factors impose a cDC1 signature in human fibroblasts.

Pathways associated with successful and unsuccessful cDC1 reprogramming

We used Monocle 3 to reconstruct the cDC1 reprogramming trajectory (25). HEFs and cDC1s were placed in the beginning and end of pseudotime, respectively (Fig. 2A-B). While d9 hiDCs were placed at the end together with cDC1s, d3 and d6 hiDCs were located in the middle highlighting the stepwise transition of single cell transcriptomes during cDC1 reprogramming. Importantly, affiliated d9 hiDCs were positioned later in pseudotime when compared to their unaffiliated counterparts, suggesting that trajectory reconstruction is capturing a successful cDC1 reprogramming path. We also observed a “dead-end” trajectory with unaffiliated hiDCs mapping closer to HEFs, suggesting that these cells fail to enter the successful reprogramming path. To infer expression dynamics and directionality of individual cells during reprogramming, we applied scVelo analysis (26) to the reprogramming trajectory. hiDC velocities are mainly aligned with the cDC1 reprogramming trajectory projected by Monocle 3 (Fig. 2C). Nevertheless, we observed that hiDCs mapping closer to the dead-end trajectory display velocities pointing towards HEFs, in agreement with previous reports describing unsuccessful reprogramming paths marked by the expression of genes associated with the original cell state (19–21). Reconstruction of gene expression dynamics using latent time showed downregulation of cell cycle genes during cDC1 reprogramming (Fig. 2D-E), suggesting that hiDCs exit cycle. We also observed enrichment in cytokine and IFN type-I and II (IFN- γ) signaling pathways later in latent time. To address differences between hiDC d9 DR $^+$ and cDC1s, we performed gene set enrichment analysis (GSEA) and observed that reprogrammed cells were enriched in IFN- γ , IFN- α , Oncostatin M, IL-6 and IFN- α signaling pathways (fig. S5A). The downregulation of cell cycle and upregulation of IFN gene signatures go in line with our previous findings in the mouse system (17). Indeed, we identified 742 genes commonly upregulated during mouse and human DC reprogramming that include genes implicated in

IFN response (fig. S5B, C), suggesting a species-conserved role for IFN signaling in cDC1 reprogramming. To map stage-specific gene changes along reprogramming, we clustered genes differentially expressed along pseudotime in 21 modules (Fig. 2F). Unaffiliated hiDCs fail to downregulate several gene modules enriched in HEFs, including modules 1, 2, 4 and 7 (unsuccessful reprogramming). Affiliated hiDCs are enriched in modules 3, 9, 13, 15 and 17 (successful reprogramming) highly expressed in cDC1s. Extraction of genes encoding surface molecules and transcriptional regulators from these modules highlighted fibroblast genes enriched in unsuccessful reprogramming (*CD248* and *PRRX1*) and DC genes upregulated in successful reprogrammed cells, including the cDC1 marker *CD226*(23) and *IRF7*(27) (Fig. 2G, figure S6A-B). Accordingly, hiDC d9 DR⁺ expressed higher levels of CD226 than hiDC d9 DR⁻ (Fig. 2H). To validate the utility of CD226 to identify cDC1-like cells, we purified CD226⁺ hiDCs d9 DR⁺ and compared their DC1 affiliation with CD226⁻ hiDC d9 DR⁺ cells. Interestingly, profiling of CD226⁺ cells resulted in increased DC1 affiliation (from 19.5% to 40.9%) (Fig. 2I), suggesting that CD226 allows the isolation of hiDCs with refined cDC1 identity. Transcription factor enrichment analysis for unsuccessful reprogramming genes identified previously described barriers to direct reprogramming, including TWIST1, TWIST2, PRRX1, PRRX2 and OSR1 (28) (fig. S6C, table S2). Interestingly, the same analysis on successful reprogramming genes reinforced the importance of PU.1, IRF8 and BATF in the establishment of successful cDC1 reprogramming gene signatures (fig. S6D). To assess whether additional regulators would enhance reprogramming, we supplemented PU.1, IRF8 and BATF3 with individual transcription factors associated with successful cDC1 reprogramming (fig. S6B, S6D, table S2) and observed that IRF7 and BATF increased cDC1 reprogramming efficiency (Fig. 2J). IRF7 is a transcriptional regulator downstream inflammatory signalling (27). BATF is highly homologous to BATF3 and was shown to compensate BATF3 during cDC1 development (29). These results suggest that cDC1 reprogramming efficiency may be increased with inflammatory signalling and the intrinsic modulation of transcription factors enriched in successful cDC1 reprogramming.

Increasing cDC1 reprogramming efficiency

We hypothesize that inflammatory cytokines could synergize with PIB to impose cDC1 identity. Thus, we added 17 hematopoietic cytokines (table S1) to the cultures 2 days after PIB induction in HEFs and measured reprogramming efficiency at day 9. IFN- γ had the most significant impact promoting 20-fold increase in CD45⁺HLA-DR⁺ cell generation ($7.9 \pm 2.2\%$ versus $0.4 \pm 0.2\%$) (Fig. 3A). Interestingly, other inflammatory cytokines also increased reprogramming efficiency, including IL-1 β (3-fold), IL-6 (2.5-fold), Oncostatin M (4-fold), TNF- α (3-fold) and IFN- β (4-fold), providing experimental validation to the single-cell analysis. Similarly to mouse DC reprogramming (17), FLT3L, IL-4 and GM-CSF used for *in vitro* differentiation of DCs from progenitors (12) or monocytes (30) did not impact reprogramming efficiency. As expected, we did not observe CD45⁺HLA-DR⁺ cells in non-transduced HEF cultures supplemented with cytokines. Considering the role of IFNs as regulators of HLA gene expression, we quantified the emergence of total CD45⁺ cells as a measure of hematopoietic commitment (fig. S7A). IFN- γ and IFN- β induced 2- and 3-fold increase in CD45⁺ cells respectively, confirming that IFN signaling facilitates DC reprogramming independently of HLA-DR activation. HiDC generation remained constant

with doses of IFN- γ ranging from 1.5 to 100 ng/ml, showing that low concentrations are effective (fig. S7B). We then tested combining IFN- γ with other inflammatory cytokines (Fig. 3B, fig. S7C-D). IFN- γ with IFN- β or IFN- α induced an additional 2.5-fold and 2-fold increase and combining the three cytokines resulted in $28.1 \pm 3.4\%$ efficiency (Fig. 3B, fig. S7C-D). Accordingly, hiDCs express genes encoding surface receptors for Type I and II IFN and TNF (fig. S7E). These data demonstrate that DC reprogramming efficiency is increased with the provision of inflammatory cytokines.

Using trajectory reconstruction of cDC1 reprogramming, we identified PU.1, IRF8 and BATF3 as drivers of successful reprogramming gene signatures. Thus, we hypothesized that enforced expression of this combination of transcription factors using a stronger constitutive promoter would increase reprogramming efficiency. We cloned the PIB polycistronic cassette followed by IRES-GFP into constitutive lentiviral backbones with multiple promoters and evaluated cDC1 reprogramming efficiency in Clec9a-tdTomato MEFs (17) (Fig. 3C). PIB overexpression driven by spleen focus-forming virus (SFFV) promoter induced superior efficiency ($46.6 \pm 16.7\%$ tdTomato $^+$ MHC-II $^+$ cells) (Fig. 3C, fig. S7F). Indeed, SFFV-driven overexpression of reprogramming factors increased efficiency of reprogramming fibroblasts to iPSCs (31). In HEFs we observed the emergence of $21.3 \pm 6.1\%$ hiDCs with SFFV overexpression (Fig. 3D). Interestingly, this system induced CD45 expression in the majority (>80%) of fibroblasts, suggesting that reprogramming is kick-started in a larger cohort of cells (Fig. 3D). We then combined SFFV-driven induction with IFN- γ , IFN- β and IFN- α and observed $76.9 \pm 11.9\%$ of hiDCs, a remarkable 190-fold increase in cDC1 reprogramming efficiency when compared to the original protocol (Fig. 3D). We also observed an increase in the absolute number of hiDCs generated with the improved protocol (Fig. 3E). Then, we evaluated the impact of anti-inflammatory cytokine signaling during cDC1 reprogramming. While IL-10 did not impact reprogramming efficiency, TGF- β reduced 2-fold (fig. S7G). Neither of the cytokines had an impact in CD40 expression. Next, we profiled hiDCs obtained with inducible (TetO-PIB) and constitutive (SFFV-PIB) with and without cytokines and used scPred for integration (Fig. 3F, table S3). Interestingly, 61.4% and 53.2% of hiDCs generated with SFFV were affiliated to DC1 lineage, with and without cytokines respectively, in contrast to only 33.4% and 22.0% generated with the inducible system. These data suggest that cytokine signaling and enforced expression of PU.1, IRF8 and BATF3 synergize for successful reprogramming, increasing both reprogramming efficiency and cDC1 identity. Commonly upregulated genes are associated with IFN signaling and antigen processing and presentation pathways, including *B2M*, *HLA-A*, *HLA-DRA*, *HLA-DPA1*, *CD74* and *NAAA* (Fig. 3G-H, fig. S8A-B). Importantly, hiDC generated with SFFV-PIB and cytokines were positioned later in pseudotime (Fig. 3I), were enriched in successful reprogramming gene signatures (Fig. 3J) and expressed higher levels of CD226, CD38 and CADM1 surface markers correlated with successful cDC1 reprogramming (fig. S8C, Table S2). Collectively, we demonstrated that scRNA-seq coupled with dimensionality reduction and trajectory inference techniques inform the dynamics of cDC1 reprogramming and identify critical pathways for establishing human cDC1 fate.

Functional human reprogrammed cDC1-like cells

DCs orchestrate adaptive immunity by uptaking and presenting antigens to T-cells. Thus, we evaluated the levels of costimulatory molecules induced upon activation with agonists for toll-like receptor 4 (TLR4) [Lipopolysaccharide (LPS)], TLR3 [Polyinosinic-polycytidylic acid (Poly I:C)] and TLR7/8 [Resiquimod (R848)] in hiDCs, required for efficient T-cell activation. While hiDCs responded to higher extent to TLR4 than cDC1s, they both upregulated co-stimulatory molecules after TLR3 or combined stimuli (Fig. 4A). To evaluate phagocytic capacity, we performed short incubation with labeled dead cells. We observed that $47.5 \pm 12.0\%$, $19.4 \pm 7.7\%$ and $10.9 \pm 3.5\%$ of hiDCs, hiDCs generated in the presence of IFN- γ , IFN- β and IFN- α (hiDC+cyt) and cDC1s, respectively, incorporated dead cell material (Fig. 4B-D, movie S1), a critical feature of cross-presenting DCs. Interestingly, we observed that CD226 $^+$ hiDCs performed better in dead cell phagocytosis when compared to CD226 $^-$ hiDCs, suggesting that CD226 marks functional hiDCs (Fig. 4E). DC maturation and phagocytosis are often inversely correlated (10). Accordingly, hiDCs generated in the presence of IFN- γ , IFN- β and IFN- α expressed higher levels of co-stimulatory molecules and showed decreased capacity to incorporate dead cells (Fig. 4A-C). To confirm that hiDCs also provide the third signal required for T-cell activation, we evaluated cytokine secretion (Fig. 4F). We first observed that hiDCs and cDC1s responded to TLR3 challenge by secreting the human cDC1-specific cytokine IFN- λ 1 (9). This comes in contrast to moDCs that were unresponsive to TLR3 agonists (32). In addition, hiDCs also responded to TLR4 and 3 by secreting IL12p70, CXCL10 and TNF- α . Moreover, we observed that IFN- γ , IFN- β and IFN- α signaling increased the magnitude of cytokine secretion. We then asked whether hiDCs cross-present antigens to CD8 $^+$ T-cells. We co-cultured HEFs, moDCs, cDC1s and hiDCs pulsed with CMV protein with CD8 $^+$ T cells isolated from CMV $^+$ donors. As readout for T-cell activation, we quantified IFN- γ secretion after co-culture (Fig. 4G). As expected, we observed that cDC1s, in contrast to moDCs or HEFs, efficiently cross-presented CMV antigens to CD8 $^+$ T cells. Strikingly, we observed that hiDCs generated with or without cytokines established the ability to cross-present antigens to CD8 $^+$ T-cells. Together, these data support that reprogrammed hiDC are functional cross-presenting DCs.

Efficient reprogramming of human adult somatic cells

The generation of cDC1s from easily accessible human cells would enable cDC1-based vaccination. Thus, we investigated the feasibility of generating hiDCs from adult human dermal fibroblast (HDFs) and mesenchymal stromal cells (MSCs). First, we observed that cDC1 reprogramming efficiency ranged from 20-35% across HDFs obtained from 3 healthy donors (Fig. 5A-B). When combined with IFN- γ , IFN- β and IFN- α , reprogramming efficiency increased ~2-fold as well as CD40 and CD80 expression (Fig. 5C). scPred analysis correctly assigned 60.6% and 59.3% of HDF-derived hiDCs generated with and without cytokines, respectively, to the DC1 subset (Fig. 5D, table S4). cDC1 identity was further supported by t-SNE visualization (Fig. 5E), expression of cDC1-specific (*C1orf54*, *NAAA* and *HLA-DPA1*) (Fig. 5F) and antigen processing and presentation genes (*CD74*, *HLA-C*, *B2M*, *PSMB9* and *TAPI*) (Fig. 5G). We then asked whether we could generate hiDCs from MSCs in xeno-free conditions. Purified MSCs from 3 donors were transduced with SFFV-PIB particles and cultured in chemically defined, serum-free X-VIVO 15 media (Fig. 5H). We observed that 60-75% of MSCs converted into hiDCs co-expressing

CD40 and CD80 (Fig. 5I-K). Interestingly, IFN- γ , IFN- β and IFN- α did not improve the generation of hiDCs from MSCs, suggesting that inflammatory cytokine signaling may facilitate cDC1 reprogramming in a cell-type specific manner. These data highlight the consistency of human cDC1 reprogramming across multiple somatic cell types and donors.

PU.1-dominant chromatin targeting capacity in cDC1 reprogramming

To shine light on molecular mechanisms underlying DC reprogramming mediated by PU.1, IRF8 and BATF3, we expressed the three reprogramming factors in combination or individually in HDFs, and performed chromatin immunoprecipitation sequencing (ChIP-seq) at early stages of reprogramming (48h, Fig. 6A). First, we observed that PU.1 showed the highest chromatin binding activity (75,593 peaks), followed by IRF8 (18,962 peaks) and BATF3 (11,505 peaks) when factors were co-expressed (Fig. 6B, table S5). Interestingly, we observed that >40% of PU.1-bound peaks were similar between individual and combined expression, suggesting that PU.1 has independent targeting capacity that is augmented when IRF8 and BATF3 are available. Accordingly, we observed increased PU.1 binding at promoter regions when expressed in combination with IRF8 and BATF3 (Fig. 6C). In sharp contrast, IRF8 and BATF3 peaks were scarce when these transcription factors were expressed individually (<3% of peaks when compared to combined expression), suggesting that IRF8 and BATF3 require cooperative binding with PU.1 to engage chromatin and induce cDC1 fate. The DC1-specific genes *C1orf54* and *ZNF366*, and *STAT1*, important for DC maturation, were targeted individually by PU.1 or the three transcription factors when combined (Fig. 6D, fig. S9A). Known and *de novo* motif prediction analysis for PU.1 peaks showed strong enrichment for PU.1 motif when expressed individually or in combination (Fig. 6E, fig. S9B). While IRF8 and BATF3 expressed individually showed enrichment in IRF and AP-1 motifs respectively, the PU.1 motif was highly enriched for these transcription factors when expressed in combination. We next explored the regulatory interactions between PU.1, IRF8 and BATF3 and observed that these cDC1-inducing factors bind each other's *loci* when co-expressed (fig. S9C), suggesting auto-regulation at the transcriptional level (fig. S9D). These data go in line with recent findings describing PU.1 as a non-classical pioneer transcription factor capable of redistributing partner transcription factors in human myeloid and lymphoid cells (33), and highlight the cooperative dynamics of the three reprogramming factors at early stages of cDC1 reprogramming.

Cooperative binding of PU.1, IRF8 and BATF3 at promoters and enhancers at open chromatin

We next investigated the overlap between PU.1, IRF8 and BATF3 chromatin targets. 5,383 genomic positions were shared between the three reprogramming factors when expressed together, representing 28% and 47% of total IRF8 and BATF3 peaks, respectively (Fig. 7A). As expected, only a residual overlap (3 genomic positions) was observed when the transcription factors were expressed individually (fig. S10A). *De novo* motif prediction for the PIB overlapping peaks showed enrichment for PU.1-IRF and BATF motifs (Fig. 7B), which also displayed some overlap and similarity (Jaccard similarity index = 0.02) (Fig. 7C). Furthermore, differential motif prediction analysis for unique and shared peaks highlighted enrichment in BATF-IRF4 motif (fig. S10B). These data suggest that PU.1, IRF8 and BATF3 interact physically. To test this hypothesis, we performed co-

immunoprecipitation (co-IP) and observed interactions between the 3 factors, highlighting an important interplay between reprogramming factors (Fig. 7D, fig. S10C). We next plotted differentially expressed genes between HDFs and hiDC d9 that were bound by at least one of the reprogramming factors and observed that they contain both downregulated fibroblast genes and upregulated cDC1-associated genes, including *SLAMF8* and *TACSTD2* (Fig. 7E, fig. S10D, E). To dissect whether PU.1, IRF8 and BATF3 binding occurs at open or closed chromatin regions, we took advantage of publicly available ChIP-seq datasets for histone marks in HDFs. PU.1, IRF8 and BATF3 co-bound sites, as well as sites bound by individual transcription factors, were mainly enriched in chromatin marks associated with active promoters and enhancers including H3K4me3, H3K4me1 and H3K27ac (Fig. 7F, fig. S10F). To better characterize PIB chromatin engagement, we used ChromHMM chromatin segmentation (34). We observed that PIB co-bound peaks were enriched mainly at promoter and enhancer regions (Fig 7G). We also observed a small fraction (12%) of peaks associated with bivalent chromatin marked either by H3K4me1, H3K4me3 and H3K27me3 or H3K4me1 and H3K27me3. Together, our data support a model where PU.1 binds mainly to active promoters and enhancers at open chromatin sites and recruits IRF8 and BATF3 to silence fibroblast genes and gradually impose the human cDC1 transcriptional program (Fig. 7H).

Discussion

In this study, we use scRNA-seq to dissect reprogramming trajectories and identify pathways associated with successful and unsuccessful cDC1 reprogramming. Overexpression of PIB imposes a cDC1-like cell fate and does not induce transcriptional programs of other DC subsets at the single-cell level. This goes in line with our previous findings, where PIB overexpression imposed a cDC1-like fate in mouse fibroblasts (17). A fraction of hiDCs did not downregulate fibroblast-specific genes and therefore did not achieve complete reprogramming. Similarly, a refractory reprogramming path sustaining fibroblast gene expression was identified in endoderm progenitor, neuronal and cardiac reprogramming (19–21). It will be interesting to test whether pharmacological inhibition or gene knock-down of transcriptional regulators associated with unsuccessful reprogramming lower barriers of cDC1 reprogramming (18) and address whether those barriers are conserved in other reprogramming systems. We used single-cell transcriptional profiling to resolve pathways associated with successful cDC1 reprogramming and improve efficiency. We identified IRF7 and BATF as additional regulators of the successful reprogramming path. Interestingly, IRF7 is a master regulator of type-I IFN-dependent immune responses (27). IFN- β signaling increased cDC1 reprogramming efficiency, pointing out to a central role of type-I IFN signaling in hiDC generation. Additionally, a BATF3-independent pathway for the generation of cDC1s in mice has been identified during infection by intracellular pathogens requiring compensation by BATF (29). Our data suggest that BATF3 and BATF may synergize molecularly during cDC1 reprogramming. Moreover, trajectory reconstruction enabled the identification of CD226, a cDC1-specific surface marker (23, 35), that allowed the isolation of hiDCs with improved functional properties. Successful cDC1 reprogramming gene signatures were also associated with the reprogramming factors. DC specification relies on different doses of PU.1 and IRF8, with the cDC1 lineage requiring

the highest of both (2). Indeed, effects downstream IRF8 were shown to be dose-dependent (36). In this study, we showed that enforced expression of PU.1, IRF8 and BATF3 using the strong SFFV promoter allowed major improvements in cDC1 reprogramming efficiency. In reprogramming, high levels of the transcription factors Ascl1 or Mef2c, Gata4 and Tbx5 are required for successful neuronal (19) or cardiomyocyte reprogramming, respectively (18). Interestingly, previous studies showed that SFFV promoter allows high transgene expression and efficient iPSCs generation (31), pointing out to a general cell fate conversion mechanism. We also identified the association of inflammatory signaling and successful cDC1 reprogramming. We confirmed synergy between extrinsic IFN- γ , IFN- β and IFN- α signaling with intrinsic expression of reprogramming factors. The cytokine cocktail may increase efficiency by inherently promoting a cDC1-specific transcriptional program or by inducing an inflammatory program that benefits cell fate conversion. Indeed, TLR3 stimulation was shown to enhance chromatin remodeling and reprogramming towards iPSCs (37), while TLR3 knock down impaired the generation of cardiomyocytes by direct reprogramming (21). As an exception, cytokines did not increase efficiency from MSCs, suggesting that reprogramming is already happening at optimal levels or that MSCs are less responsive to inflammatory stimuli. Collectively, single-cell analysis revealed the gradual and asynchronous nature of exclusive cDC1 reprogramming, highlighted a successful reprogramming path with associated pathways and factors that allowed a 190-fold increase in reprogramming efficiency. We can envision that a similar single-cell approach can be applied to other reprogramming systems where translation to the human system is limited by low efficiency.

The rarity of natural cDC1s has limited genomic location studies in human cells. Nevertheless, studies in mice have shown that IRF8 interacts with ETS and AP-1 factors during DC ontogeny. For instance, IRF8 is recruited to target sites via the interaction with PU.1 or other ETS transcription factors, due to the low affinity of IRF8 to interferon-response elements (38). Moreover, AP-1 TFs, including BATF3, were shown to interact with IRF4 and IRF8 at AP-1-IRF composite sites (29). Here, our chromatin immunoprecipitation and protein interaction studies show that the three transcription factors interact and form a "cDC1 reprogramming complex" at the early stages of cDC1 reprogramming. Importantly, these data imply that induction of human cDC1 identity involves direct interplay between the three transcription factors. Accordingly, it was recently reported that IRF8 binding at mouse cDC1-specific genes is enriched in both AP1-IRF and ETS-IRF composite elements (39). Chromatin engagement models of transcription factor-mediated reprogramming have been suggested to rely on pioneer factor capacity of binding closed chromatin and to directly induce target cell-type gene expression programs (40) or to depend on the cooperative interaction enabling the inactivation of the starting cell-type enhancers and the gradual induction of target cell-type genes (41). Our cDC1 reprogramming data support a cooperative and step-wise, immune induction model (41, 42). PU.1 functions as a non-classical pioneer transcription factor as it binds to promoters and enhancers at open chromatin regions recruiting IRF8 and BATF3. In CD4 $^{+}$ T cells, reorganization of chromatin relies on BATF pioneer function coupled with ETS1-dependent recruitment of CTCF (43). In cDC1 reprogramming however, BATF3 shows an almost complete dependency on PU.1 and IRF8 expression for chromatin binding. This suggests that either BATF and BATF3

utilize different chromatin engagement mechanisms or in cDC1 specification, BATF3 may cooperate with PU.1 for CTCF recruitment and chromatin looping. In the future, it will be interesting to further map chromatin binding dependencies of each transcription factor by profiling engagement in pairs during cDC1 reprogramming. We believe cDC1 reprogramming provides a unique system to explore molecular mechanisms underlying human cDC1 specification.

The lack of methods allowing the generation of a pure population of functional cDC1-like cells has also been a major bottleneck in the clinical development of cDC1-based cancer vaccines (14). Classically, moDCs were used to generate DC vaccines due to the ease at obtaining sufficient number of cells from peripheral blood (44). However, moDCs show functional deficiencies, including their limited T-cell priming ability, that may explain suboptimal clinical responses (45). Here, we show that hiDCs express co-stimulatory molecules and secrete inflammatory cytokines, i.e. IFN- λ , IL12p70 and CXCL10 upon TLR stimulation. IFN- λ secretion by tumor-associated cDC1s was shown to induce IL12p70 and CXCL10 secretion, involved in the recruitment and activation of NK and T cells (9, 46). Indeed, expression of these cytokines within the tumor is correlated with favorable clinical outcome (9). Both natural cDC1s and hiDCs responded to TLR3 stimulation and we also observed that hiDCs were responsive to TLR4 stimulation. Accordingly, cDC1s differentiated from CD34 $^{+}$ hematopoietic progenitors, pointing out to a general feature of *in vitro* generated cDC1-like cells (12). In the future, it will be interesting to investigate whether this functional difference confers a functional advantage to hiDCs in driving antigen-specific immune responses. We show that hiDCs uptake dead cells, process and cross-present antigens to CD8 $^{+}$ T-cells, which supports cDC1 affiliation at a functional level. Methods to derive cDC1-like cells from BM and iPSC cultures are laborious, time consuming, require feeder layers and yield a mixture of different DC subtypes (8, 11–13). cDC1 reprogramming takes up to 9 days, is robust, reproducible from different donors, does not require feeder layers or isolation and expansion of CD34 $^{+}$ progenitors and can be readily adapted to good manufacturing practices (GMP). Nonetheless, cDC1 reprogramming does not transit through an expandable cell state, which limits the absolute number of generated cDC1-like cells. This limitation may be surpassed in the future by up-scaling the number of input cells for reprogramming and by exploring additional reprogramming entities, i.e. small molecules and microRNAs, to allow near-deterministic cDC1 induction (47). In addition, an important future consideration will be the dose and timing for cytokine exposure for optimal generation of cDC1s. Indeed, we showed that hiDCs generated in the presence of IFN- γ , IFN- β and IFN- α acquire a mature phenotype characterized by high expression of co-stimulatory molecules and reduced dead cell engulfment capacity, which might limit the therapeutic potential of hiDCs. Finally, we showed that PIB allows cDC1 reprogramming from different starting cell types, demonstrating cross-species and cross-cell type conservation of minimal transcription factor networks underlying the cDC1 lineage, potentially enabling cDC1 specification from a broad range of cell-types. This was also observed in other direct reprogramming processes including hemogenic, neuronal and hepatic (16, 48). We envision to use our network of three transcription factors for the “forward programming” of iPSCs into cDC1 or to directly convert other human somatic cells such as PBMCs, monocytes or even tumour cells to promote presentation of their

own (neo)antigens. Thus, our study provides the foundation for the systematic comparison of hiDCs generated from multiple human cell-types to available *in vitro* sources of human cDC1-like cells.

Overall, we demonstrated that PU.1, IRF8 and BATF3 impose cDC1 fate in human somatic cell types, providing a tractable system to study human cDC1 specification and function. We provided evidence that human antigen cross-presenting cells can be induced by direct reprogramming, supporting the generation of potent patient-specific cDC1s for immunotherapy.

Materials and Methods

Study Design

This study aimed to investigate the single-cell transcriptional dynamics during cDC1 reprogramming of human fibroblasts, dissecting factors and pathways triggered during successful reprogramming to optimize the generation of human functional cDC1s. We also aimed to provide mechanistic insights into the chromatin engagement of the reprogramming factors to impose cDC1 fate. For each experiment, the number of biological replicates and statistical details are described in figure legends.

Viral transduction and reprogramming

HEFs, HDFs and Clec9a-tdTomato MEFs were seeded at a density of 40,000 cells per well and MSCs at a density of 50,000 cells per well on 0.1% gelatin coated 6-well plates. On the following day, cells were incubated overnight with either a ratio of 1:1 TetO-PIB and M2rtTA, SFFV-PIB-GFP or SFFV-GFP lentiviral particles in media supplemented with 8 µg/ml polybrene. Cells were transduced overnight twice in consecutive days and media replaced in between. After the second transduction, media was replaced by normal growth media (day 0). When using TetO-PIB, media was supplemented with Dox (1 µg/ml). Media was changed every 2-3 days for the duration of cultures. When stated, media was supplemented with LPS (100 ng/ml, Enzo), Poly I:C (25 µg/ml, InvivoGen) and R848 (3 µg/ml, InvivoGen) overnight. When stated, cytokines were added at day 2 and kept for the duration of cultures; cytokine concentrations used in this study as well as antibodies, cell lines and plasmids are listed in Table S1. For reprogramming in xeno-free conditions, MSCs were cultured in X-Vivo 15 (Lonza) after transduction and media changed every 2-3 days for the duration of cell cultures.

Single-cell RNA sequencing

HEFs, hiDCs at day 3, 6 and 9 (CD45⁺HLA-DR⁻ and CD45⁺HLA-DR⁺), cDC1s, cDC2s and pDCs from peripheral blood (from 3 individual donors) were FACS sorted for scRNA-seq. Purified cells were loaded on a 10× Chromium (10× Genomics) according to manufacturer's protocol. scRNA-seq indexed libraries were prepared using Chromium Single Cell 3' v2 and v3 Reagent Kit (10× Genomics) according to manufacturer's protocol. hiDCs at day 9 reprogrammed in the presence and absence of cytokines from HEFs and HDFs and CD45⁺HLA-DR⁺CD226⁺ hiDCs were also profiled. Library quantification and quality assessment was determined using Agilent Bioanalyzer using the High Sensitivity

DNA analysis kit (Agilent). Indexed libraries were pooled at equimolarity and sequenced on an Illumina NextSeq 500. Coverage of approximately 130,000 reads per single cell was obtained. Details regarding scRNA-seq data analysis can be found in supplementary materials.

ChIP sequencing

HDFs were transduced with TetO-PIB or vectors encoding individual factors (TetO-PU.1, TetO-IRF8, or TetO-BATF3) and M2rtTA. Transduced HDFs were expanded and ChIP was performed 48 hours after the addition of Dox using antibodies for human PU.1, human IRF8 and human BATF3 (table S1). Details regarding ChIP-seq and analysis can be found in supplementary materials.

Human antigen cross-presentation assay

HEFs, moDCs, magnetic-activated cell sorting (MACS)-enriched cDC1s (see supplementary methods) and hiDCs at reprogramming day 8 were stimulated with LPS (3 ng/ml), Poly I:C (25 µg/ml) and R848 (3 ng/ml). After overnight stimulation, cells were washed in PBS containing 2% FBS and pulsed with 2 µl/ml of CMV protein (Miltenyi Biotec). After 3 hours, cells were washed and co-cultured with MACS-enriched CD8⁺ T cells isolated from CMV-seropositive donors. CMV positivity was verified by flow cytometry using a CMV Dextramer (ImmuDex). 1x10⁵ CD8⁺ T cells and 5x10⁴ DCs were co-cultured in 96-well plates in 200µl of X-VIVO 15. After 24 h, T-cell activation was measured by quantifying IFN-γ levels in the supernatants using ELISA (BD). Absorbance was read at 490 nm in a GloMax Discover Microplate Reader (Promega).

Statistical analysis

Comparisons among groups were performed using one-way ANOVA followed by Dunnett multiple comparisons test with Prism 9 software (GraphPad). P-values are shown when relevant (*p<0.05; **p<0.01, ***p<0.001, ****p<0.0001, ns - non-significant).

Supplementary Material

Refer to Web version on PubMed Central for supplementary material.

Acknowledgments

We thank the members of the Pereira laboratory for useful discussions. We thank Axel Schambach and Christopher Baum (Institute of Experimental Hematology, Hannover, Germany) for sharing the plasmids pRRRL.PPT.SF.GFPpre, pRRRL.PPT.PGK.GFPpre and pRRRL.PPT.EFS.GFPpre. We thank Zaal Kokaia, Henrik Ahlenius and Ella Quist (LSCC, Lund, Sweden) for providing HEFs (ethical permit: Dnr 6.1.8-2887/2017). We also thank healthy donors and the center for Clinical Immunology and Transfusion Medicine at Skåne University Hospital for providing leukoconcentrates (ethical permit: 2020:14). We thank Center for Translational Genomics and Clinical Genomics Lund, SciLifeLab for providing sequencing services. We would also like to thank Lund University Bioimaging Center and Lund Stem Cell Center FACS Facility for SEM and FACS assistance. We thank Sonja Buschow (Erasmus MC, Rotterdam, The Netherlands) for helpful discussions.

Funding

This project has received funding from the European Research Council (ERC) under the European Union's Horizon 2020 research and innovation programme (Grant agreement No. 866448). This project was co-funded by Cancerfonden (CAN 2017/745), the Swedish research council (2018-02042), NovoNordisk Fonden (0056527)

and FCT (CENTRO-01-0145-FEDER-030013). The Knut and Alice Wallenberg foundation, the Medical Faculty at Lund University and Region Skåne are acknowledged for generous financial support. F.F.R and A.G.F. are supported by FCT doctoral fellowships (SFRH/BD/130845/2017 and SFRH/BD/133233/2017).

Data and materials availability

The data reported in this paper are tabulated in the Supplementary Materials and deposited in the Gene Expression Omnibus database under accession number GSE162650. Requests for plasmids should be directed to Asgard Therapeutics (www.asgardthx.com).

References

1. Cabeza-Cabrero M, Cardoso A, Minutti CM, Pereira da Costa M, Reis ESC. Dendritic Cells Revisited. *Annual review of immunology*. 2021; 39: 131–166.
2. Lee J, Zhou YJ, Ma W, Zhang W, Aljoufi A, Luh T, Lucero K, Liang D, Thomsen M, Bhagat G, Shen Y, Liu K. Lineage specification of human dendritic cells is marked by IRF8 expression in hematopoietic stem cells and multipotent progenitors. *Nature immunology*. 2017; 18: 877–888. [PubMed: 28650480]
3. Poulin LF, Reyal Y, Uronen-Hansson H, Schraml BU, Sancho D, Murphy KM, Hakansson UK, Moita LF, Agace WW, Bonnet D, Reis e Sousa C. DNGR-1 is a specific and universal marker of mouse and human Batf3-dependent dendritic cells in lymphoid and nonlymphoid tissues. *Blood*. 2012; 119: 6052–6062. [PubMed: 22442345]
4. Schönheit J, Kuhl C, Marie Gebhardt L, Francisco F, Klett P, Riemke M, Scheller G, Huang R, Naumann A, Leutz C, Stocking C, et al. PU.1 Level-Directed Chromatin Structure Remodeling at the Irf8 Gene Drives Dendritic Cell Commitment. *Cell reports*. 2013; 3: 1617–1628. [PubMed: 23623495]
5. Grajales-Reyes GE, Iwata A, Albring J, Wu X, Tussiwand R, Kc W, Kretzer NM, Briseno CG, Durai V, Bagadia P, Haldar M, et al. Batf3 maintains autoactivation of Irf8 for commitment of a CD8alpha(+) conventional DC clonogenic progenitor. *Nature immunology*. 2015; 16: 708–717. [PubMed: 26054719]
6. Durai V, Bagadia P, Granja JM, Satpathy AT, Kulkarni DH, Davidson JTt, Wu R, Patel SJ, Iwata A, Liu TT, Huang X, et al. Cryptic activation of an Irf8 enhancer governs cDC1 fate specification. *Nature immunology*. 2019; 20: 1161–1173. [PubMed: 31406378]
7. Villani A-C, Satija R, Reynolds G, Sarkizova S, Shekhar K, Fletcher J, Griesbeck M, Butler A, Zheng S, Lazo S, Jardine L, et al. Single-cell RNA-seq reveals new types of human blood dendritic cells, monocytes, and progenitors. *Science (New York, N.Y.)*. 2017; 356
8. Poulin LF, Salio M, Griessinger E, Anjos-Afonso F, Craciun L, Chen JL, Keller AM, Joffre O, Zelenay S, Nye E, Le Moine A, et al. Characterization of human DNGR-1+ BDCA3+ leukocytes as putative equivalents of mouse CD8alpha+ dendritic cells. *The Journal of experimental medicine*. 2010; 207: 1261–1271. [PubMed: 20479117]
9. Hubert M, Gobbini E, Couillault C, Manh TV, Doffin AC, Berhet J, Rodriguez C, Ollion V, Kielbassa J, Sajous C, Treilleux I, et al. IFN-III is selectively produced by cDC1 and predicts good clinical outcome in breast cancer. *Science immunology*. 2020; 5
10. Broz ML, Binnewies M, Boldajipour B, Amanda Nelson E, Joshua Pollack L, David Erle J, Barczak A, Michael Rosenblum D, Daud A, Diane Barber L, Amigorena S, et al. Dissecting the Tumor Myeloid Compartment Reveals Rare Activating Antigen-Presenting Cells Critical for T Cell Immunity. *Cancer cell*. 2014; 26: 638–652. [PubMed: 25446897]
11. Kirkling ME, Cytlak U, Lau CM, Lewis KL, Resteu A, Khodadadi-Jamayran A, Siebel CW, Salmon H, Merad M, Tsirigos A, Collin M, et al. Notch Signaling Facilitates In Vitro Generation of Cross-Presenting Classical Dendritic Cells. *Cell reports*. 2018; 23: 3658–3672. e3656 [PubMed: 29925006]
12. Balan S, Arnold-Schrauf C, Abbas A, Couespel N, Savoret J, Imperatore F, Villani AC, Vu Manh TP, Bhardwaj N, Dalod M. Large-Scale Human Dendritic Cell Differentiation Revealing

- Notch-Dependent Lineage Bifurcation and Heterogeneity. *Cell reports*. 2018; 24: 1902–1915. e1906 [PubMed: 30110645]
13. Sontag S, Förster M, Qin J, Wanek P, Mitzka S, Schüler HM, Koschmieder S, Rose-John S, Seré K, Zenke M. Modelling IRF8 Deficient Human Hematopoiesis and Dendritic Cell Development with Engineered iPS Cells. *Stem cells (Dayton, Ohio)*. 2017; 35: 898–908.
14. Saxena M, Bhardwaj N. Re-Emergence of Dendritic Cell Vaccines for Cancer Treatment. *Trends in cancer*. 2018; 4: 119–137. [PubMed: 29458962]
15. Zimmermannova O, Caiado I, Ferreira AG, Pereira CF. Cell Fate Reprogramming in the Era of Cancer Immunotherapy. *Frontiers in immunology*. 2021; 12 714822 [PubMed: 34367185]
16. Wang H, Yang Y, Liu J, Qian L. Direct cell reprogramming: approaches, mechanisms and progress. *Nature reviews. Molecular cell biology*. 2021. 410–424. [PubMed: 33619373]
17. Rosa FF, Pires CF, Kurochkin I, Gomes AM, Ferreira AG, Palma LG, Shaiv K, Solanas L, Azenha C, Papatsenko D, Schulz O, et al. Direct Reprogramming of Fibroblasts into Antigen-Presenting Dendritic Cells. *Science immunology*. 2018; 3 (30)
18. Liu Z, Wang L, Welch JD, Ma H, Zhou Y, Vaseghi HR, Yu S, Wall JB, Alimohamadi S, Zheng M, Yin C, et al. Single-cell transcriptomics reconstructs fate conversion from fibroblast to cardiomyocyte. *Nature*. 2017; 551: 100–104. [PubMed: 29072293]
19. Treutlein B, Lee QY, Camp JG, Mall M, Koh W, Shariati SAM, Sim S, Neff NF, Skotheim JM, Wernig M, Quake SR. Quake, Dissecting direct reprogramming from fibroblast to neuron using single-cell RNA-seq. *Nature*. 2016; 534: 391–395. [PubMed: 27281220]
20. Biddy BA, Kong W, Kamimoto K, Guo C, Waye SE, Sun T, Morris SA. Single cell mapping of lineage and identity in direct reprogramming. *Nature*. 2018; 564: 219–224. [PubMed: 30518857]
21. Zhou Y, Liu Z, Welch JD, Gao X, Wang L, Garbutt T, Keepers B, Ma H, Prins JF, Shen W, Liu J, et al. Single-Cell Transcriptomic Analyses of Cell Fate Transitions during Human Cardiac Reprogramming. *Cell stem cell*. 2019; 25: 149–164. e149 [PubMed: 31230860]
22. Alquicira-Hernandez J, Sathe A, Ji HP, Nguyen Q, Powell JE. scPred: accurate supervised method for cell-type classification from single-cell RNA-seq data. *Genome biology*. 2019; 20
23. Heidkamp GF, Sander J, Lehmann CHK, Heger L, Eissing N, Baranska A, Lühr A, Hoffmann A, Reimer KC, Lux A, Söder S, et al. Human lymphoid organ dendritic cell identity is predominantly dictated by ontogeny, not tissue microenvironment. *Science immunology*. 2016; 1
24. See P, Dutertre CA, Chen J, Günther P, McGovern N, Irac SE, Gunawan M, Beyer M, Händler K, Duan K, Sumatoh HRB, et al. Mapping the human DC lineage through the integration of high-dimensional techniques. *Science (New York, N.Y.)*. 2017; 356
25. Cao J, Spielmann M, Qiu X, Huang X, Ibrahim DM, Hill AJ, Zhang F, Mundlos S, Christiansen L, Steemers FJ, Trapnell C, et al. The single-cell transcriptional landscape of mammalian organogenesis. *Nature*. 2019; 566: 496–502. [PubMed: 30787437]
26. Bergen V, Lange M, Peidli S, Wolf FA, Theis FJ. Generalizing RNA velocity to transient cell states through dynamical modeling. *Nature biotechnology*. 2020.
27. Honda K, Yanai H, Negishi H, Asagiri M, Sato M, Mizutani T, Shimada N, Ohba Y, Takaoka A, Yoshida N, Taniguchi T. IRF-7 is the master regulator of type-I interferon-dependent immune responses. *Nature*. 2005; 434: 772–777. [PubMed: 15800576]
28. Tomaru Y, Hasegawa R, Suzuki T, Sato T, Kubosaki A, Suzuki M, Kawaji H, Forrest AR, Hayashizaki Y, Shin JW, Suzuki H. A transient disruption of fibroblastic transcriptional regulatory network facilitates trans-differentiation. *Nucleic acids research*. 2014; 42: 8905–8913. [PubMed: 25013174]
29. Tussiwand R, Lee WL, Murphy TL, Mashayekhi M, Kc W, Albring JC, Rotondo JA, Edelson BT, Kretzer NM, Wu X, Weiss LA, et al. Compensatory dendritic cell development mediated by BATF-IRF interactions. *Nature*. 2012; 490: 502–507. [PubMed: 22992524]
30. Chapuis F, Rosenzwajg M, Yagello M, Ekman M, Biberfeld P, Gluckman JC. Differentiation of human dendritic cells from monocytes in vitro. *European journal of immunology*. 1997; 27: 431–441. [PubMed: 9045914]
31. Warlich E, Kuehle J, Cantz T, Brugman MH, Maetzig T, Galla M, Filipczyk AA, Halle S, Klump H, Scholer HR, Baum C, et al. Lentiviral vector design and imaging approaches to visualize the

- early stages of cellular reprogramming. *Molecular therapy : the journal of the American Society of Gene Therapy*. 2011; 19: 782–789. [PubMed: 21285961]
32. Lauterbach H, Bathke B, Gilles S, Traidl-Hoffmann C, Luber CA, Fejer G, Freudenberg MA, Davey GM, Vremec D, Kallies A, Wu L, et al. Mouse CD8alpha⁺ DCs and human BDCA3⁺ DCs are major producers of IFN-lambda in response to poly IC. *The Journal of experimental medicine*. 2010; 207: 2703–2717. [PubMed: 20975040]
 33. Minderjahn J, Schmidt A, Fuchs A, Schill R, Raithel J, Babina M, Schmidl C, Gebhard C, Schmidhofer S, Mendes K, Ratermann A, et al. Mechanisms governing the pioneering and redistribution capabilities of the non-classical pioneer PU.1. *Nature communications*. 2020; 11
 34. Ernst J, Kellis M. ChromHMM: automating chromatin-state discovery and characterization. *Nature methods*. 2012; 9: 215–216. [PubMed: 22373907]
 35. Dutertre CA, Becht E, Irac SE, Khalilnezhad A, Narang V, Khalilnezhad S, Ng PY, van den Hoogen LL, Leong JY, Lee B, Chevrier M, et al. Single-Cell Analysis of Human Mononuclear Phagocytes Reveals Subset-Defining Markers and Identifies Circulating Inflammatory Dendritic Cells. *Immunity*. 2019; 51: 573–589. e578 [PubMed: 31474513]
 36. Cytlak U, Resteu A, Pagan S, Green K, Milne P, Maisuria S, McDonald D, Hulme G, Filby A, Carpenter B, Queen R, et al. Differential IRF8 Transcription Factor Requirement Defines Two Pathways of Dendritic Cell Development in Humans. *Immunity*. 2020; 53: 353–370. e358 [PubMed: 32735845]
 37. Lee J, Sayed N, Hunter A, Au KF, Wong WH, Mocarski ES, Pera RR, Yakubov E, Cooke JP. Activation of innate immunity is required for efficient nuclear reprogramming. *Cell*. 2012; 151: 547–558. [PubMed: 23101625]
 38. Murphy TL, Tussiwand R, Murphy KM. Specificity through cooperation: BATF–IRF interactions control immune-regulatory networks. *Nature Reviews Immunology*. 2013; 13: 499–509.
 39. Kim S, Bagadia P, Anderson DA 3rd, Liu TT, Huang X, Theisen DJ, O'Connor KW, Ohara RA, Iwata A, Murphy TL, Murphy KM. High Amount of Transcription Factor IRF8 Engages AP1-IRF Composite Elements in Enhancers to Direct Type 1 Conventional Dendritic Cell Identity. *Immunity*. 2020; 53: 759–774. e759 [PubMed: 32795402]
 40. Soufi A, Donahue G, Zaret KS. Facilitators and impediments of the pluripotency reprogramming factors' initial engagement with the genome. *Cell*. 2012; 151: 994–1004. [PubMed: 23159369]
 41. Chronis C, Fiziev P, Papp B, Butz S, Bonora G, Sabri S, Ernst J, Plath K. Cooperative Binding of Transcription Factors Orchestrates Reprogramming. *Cell*. 2017; 168: 442–459. e420 [PubMed: 28111071]
 42. Gomes AM, Kurochkin I, Chang B, Daniel M, Law K, Satija N, Lachmann A, Wang Z, Ferreira L, Ma'ayan A, Chen BK, et al. Cooperative Transcription Factor Induction Mediates Hemogenic Reprogramming. *Cell reports*. 2018; 25: 2821–2835. e2827 [PubMed: 30517869]
 43. Pham D, Moseley CE, Gao M, Savic D, Winstead CJ, Sun M, Kee BL, Myers RM, Weaver CT, Hatton RD. Batf Pioneers the Reorganization of Chromatin in Developing Effector T Cells via Ets1-Dependent Recruitment of Ctcf. *Cell reports*. 2019; 29: 1203–1220. e1207 [PubMed: 31665634]
 44. Perez CR, De Palma M. Engineering dendritic cell vaccines to improve cancer immunotherapy. *Nature communications*. 2019; 10
 45. Osugi Y, Vuckovic S, Hart DN. Myeloid blood CD11c(+) dendritic cells and monocyte-derived dendritic cells differ in their ability to stimulate T lymphocytes. *Blood*. 2002; 100: 2858–2866. [PubMed: 12351396]
 46. Bronger H, Singer J, Windmüller C, Reuning U, Zech D, Delbridge C, Dorn J, Kiechle M, Schmalfeldt B, Schmitt M, Avril S. CXCL9 and CXCL10 predict survival and are regulated by cyclooxygenase inhibition in advanced serous ovarian cancer. *British journal of cancer*. 2016; 115: 553–563. [PubMed: 27490802]
 47. Babos KN, Galloway KE, Kisler K, Zitting M, Li Y, Shi Y, Quintino B, Chow RH, Zlokovic BV, Ichida JK. Mitigating Antagonism between Transcription and Proliferation Allows Near-Deterministic Cellular Reprogramming. *Cell stem cell*. 2019; 25: 486–500. e489 [PubMed: 31523028]

48. Pires CF, Rosa FF, Kurochkin I, Pereira C-F. Understanding and Modulating Immunity With Cell Reprogramming. *Frontiers in immunology*. 2019; 10:2809 [PubMed: 31921109]

One Sentence Summary

Programming functional human cDC1s

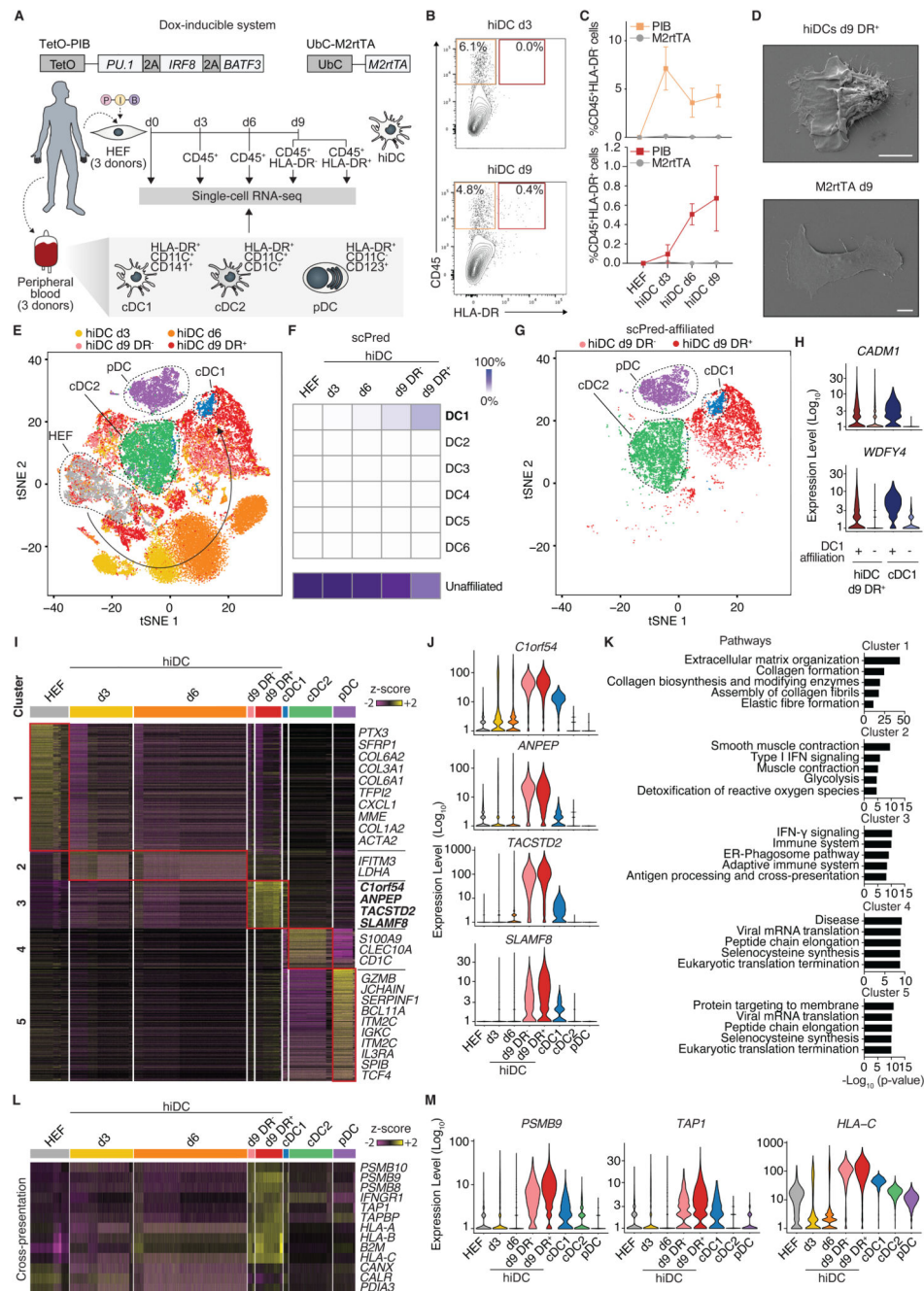


Fig. 1. PU.1, IRF8 and BATF3 induce global DC1 gene expression program in human fibroblasts.

(A) HEF were co-transduced with Dox-inducible lentiviral particles encoding M2rtTA (UbC-M2rtTA) and PU.1, IRF8 and BATF3 (PIB, TetO-PIB). Purified PIB-transduced HEFs (hiDC) were profiled by single-cell RNA-seq at day 3 (CD45⁺), day 6 (CD45⁺) and day 9 (CD45⁺HLA-DR⁻, hiDC d9 DR⁻; CD45⁺HLA-DR⁺, hiDC d9 DR⁺). HEF and peripheral blood cDC1 (HLA-DR⁺CD11C⁺CD141⁺), DC2 (HLA-DR⁺CD11C⁺CD141⁻CD1C⁺) and pDC cells (HLA-DR⁺CD11C⁺CD123⁺) were included as controls. **(B)** Flow cytometry analysis of hiDCs at day 3 and 9 after addition of Dox. **(C)** Kinetics of hiDC d9 DR⁻ cells. **(D)** Electron microscopy images of hiDCs d9 DR⁺ and M2rtTA d9. **(E)** tSNE plot of hiDCs. **(F)** scPred scores for various DC types. **(G)** tSNE plot of hiDCs with scPred-affiliated markers. **(H)** Expression levels of CADM1 and WDFY4. **(I)** Heatmap of gene expression z-scores. **(J)** Violin plots of expression levels for C1orf54, ANPEP, TACSTD2, SLAMF8, and SLAMF9. **(K)** Pathway enrichment for clusters 1-5. **(L)** Heatmap of gene expression z-scores for cross-presentation. **(M)** Violin plots for PSMB9, TAP1, and HLA-C.

(top) and hiDC d9 DR⁺ (bottom) cell emergence (n=5-8, mean ± SD). **(D)** Scanning electron microscopy of hiDCs and M2rtTA control at day 9. Scale bars, 10 µm. **(E)** t-SNE plot of single-cell transcriptomes showing 45,870 single cells. **(F)** Integration of single-cell data with published DC subset data (DC1-DC6 (7)) using scPred (22). Heat map shows the percentage of single cells affiliated to DC1-DC6 subsets or unaffiliated. **(G)** t-SNE of single cells affiliated by scPred. **(H)** Violin plots showing gene expression distribution of cDC1-specific genes in hiDCs d9 and cDC1s. Log values of gene counts are shown. **(I)** Heat map showing differentially expressed genes across profiled populations and grouped in 5 clusters. **(J)** Violin plots showing expression distribution of genes selected from cluster 3. **(K)** Top five Reactome pathway enrichment analysis for each gene cluster using Enrichr. **(L)** Heat map and **(M)** violin plots showing expression of genes associated with antigen cross-presentation pathway across profiled populations.

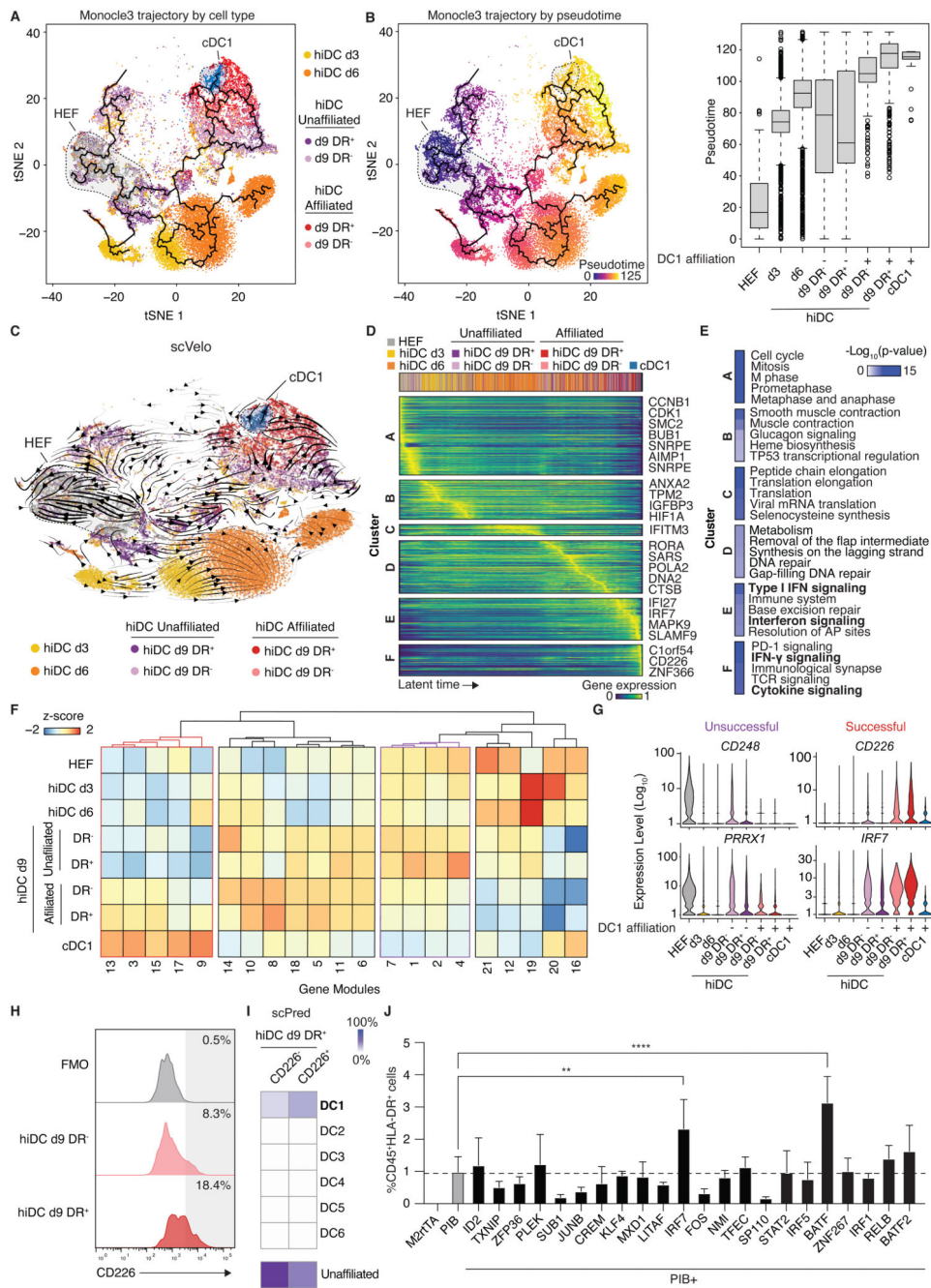


Fig. 2. Pseudo-temporal ordering of single cells highlights gene modules and pathways associated with successful and unsuccessful cDC1 reprogramming.

(A) Monocle 3 reconstruction of single-cell trajectories for HEF, hiDC at day 3, day 6, day 9 (d9 DR⁻ and d9 DR⁺) unaffiliated or affiliated with DC1 and scPred-filtered cDC1s. (B) cDC1 reprogramming trajectory colored by relative trajectory position (pseudotime) (left). Whisker box plots showing pseudotime distribution by cell type (right). (C) scVelo (26) single-cell velocities visualized in a tSNE plot. Arrows indicate direction and thickness indicates speed along cDC1 reprogramming trajectory. (D) Heat map highlighting 6 gene

clusters (A-F) showing gene expression dynamics along scVelo latent time. (E) Top 5 Reactome pathway enrichment analysis of clusters A-F. (F) Heat map showing mean expression values of gene modules by cell-type differentially expressed along cDC1 reprogramming trajectory. (G) Violin plots showing expression distribution of genes associated with unsuccessful and successful DC reprogramming. Log values of gene counts are shown. (H) Flow cytometry analysis of CD226 expression in d9 DR⁻ and d9 DR⁺ hiDCs. (I) Classification with published DC subset data (DC1-DC6 (7)) using scPred (22). (J) Percentage of CD45⁺HLA-DR⁺ cells at day 9 generated by co-transduction of Dox-inducible PIB with indicated transcription factors (n=4, mean ± SD). M2rtTA- and PIB-transduced cells were included as controls. ** p<0.005; **** p<0.00005.

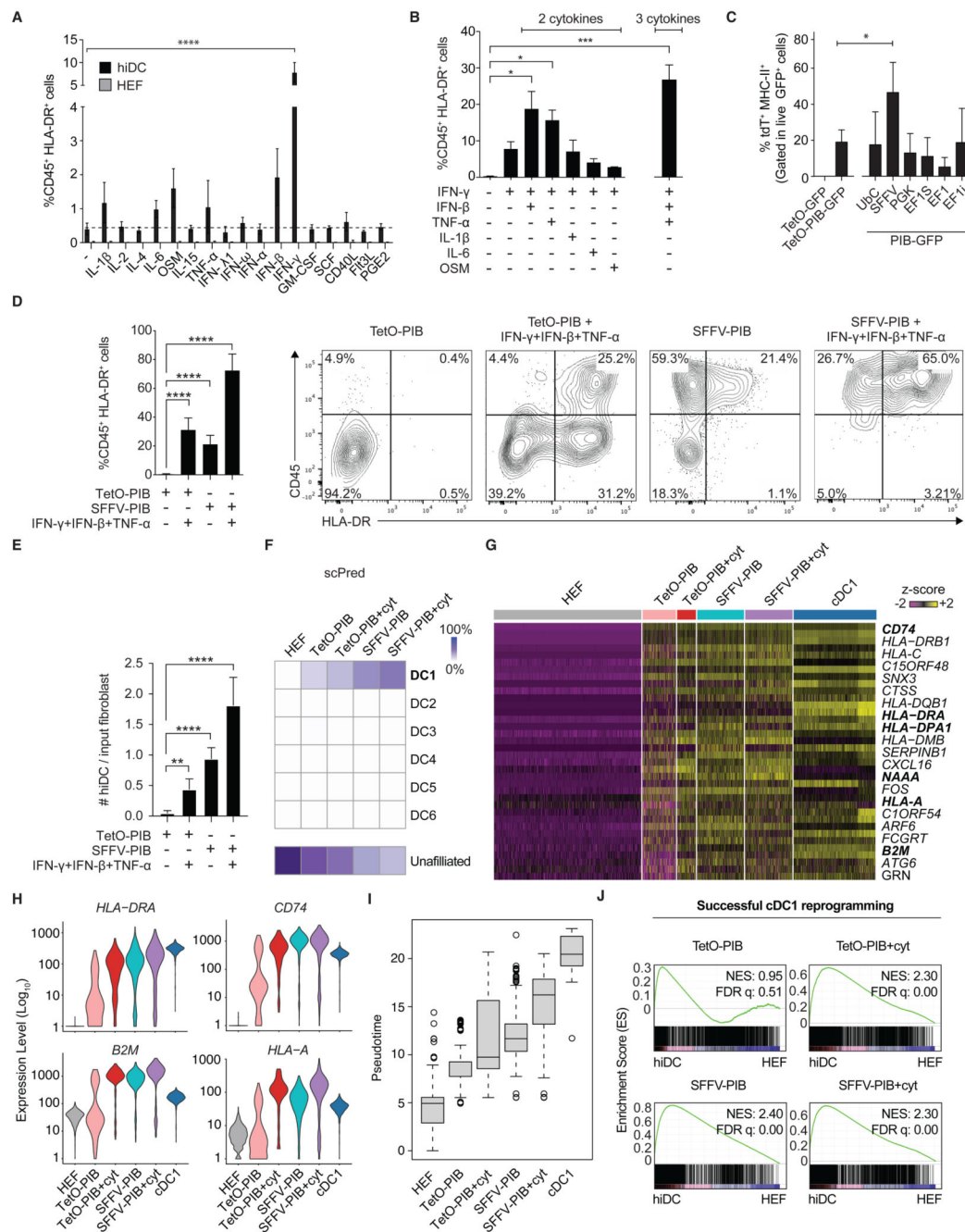


Fig. 3. Inflammatory cytokine signaling and enforced expression of transcription factors enable human cDC1 reprogramming at high efficiency.

(A) Quantification of hiDCs (CD45⁺HLA-DR⁺) at day 9 obtained in the presence of single cytokines and (B) combinations of two or three cytokines. Non-transduced HEF were included as control (n=2-5, mean \pm SD). (C) Quantification of reprogrammed cells (tdT⁺MHC-II⁺ in live GFP⁺ cells) obtained by transducing Clec9a-tdTomato (tdT) reporter mouse embryonic fibroblasts with lentiviral particles encoding GFP and PIB driven by Dox-inducible (TetO) or constitutive promoters (UbC, SFFV, PGK, EF1S, EF1 and EF1i

promoters). **(D)** Quantification of hiDCs at day 9 generated with TetO-PIB or SFFV-PIB, in the presence or absence of IFN- γ , IFN- β and IFN- α (n=3-9, mean \pm SD). **(E)** Quantification of hiDC yield after 9 days per input fibroblast. **(F)** hiDCs at day 9 generated in the four conditions were FACS sorted and profiled by scRNA-seq. Heat map shows the percentage of single cells affiliated to the DC1-DC6 subsets (7) by scPred (22). **(G)** Heat map showing relative expression of genes commonly upregulated in hiDCs in the four conditions and in cDC1s. **(H)** Violin plots showing expression distribution of antigen-presentation genes. Log values of gene counts are shown. **(I)** Single-cell distribution along the cDC1 reprogramming pseudotime by condition. **(J)** GSEA for successful cDC1 reprogramming (genes included in modules 13, 3, 15, 17, and 9) between hiDC day 9 and HEF. Normalized enrichment score (NES) and False discovery rate (FDR) q-values are shown. * p<0.05; ** p<0.005; *** p<0.0005; **** p<0.00005.

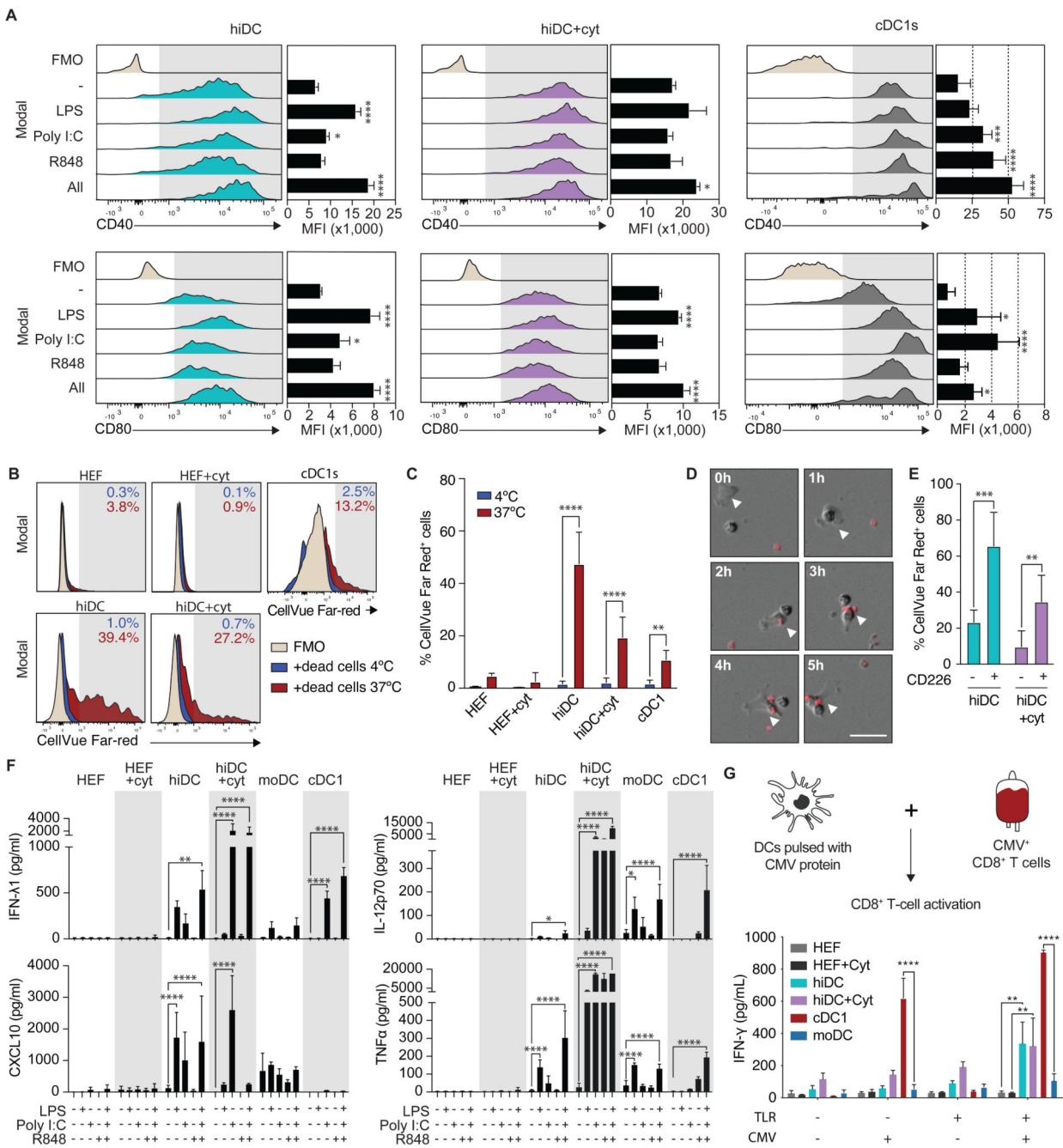


Fig. 4. Optimized DC reprogramming protocol allows generation of functional human cDC1-like cells.

(A) Median fluorescence intensity (MFI) of CD40 and CD80 expression in hiDCs (CD45⁺HLA-DR⁺) at day 9 generated with SFFV-PIB in the absence or presence of IFN- γ , IFN- β and IFN- α (hiDC+cyt) and in peripheral blood CD141⁺CLEC9A⁺ cDC1. Cells were stimulated overnight with TLR agonists LPS, Poly I:C, R848 or the three combined (All) (n=3-7, mean \pm SD). (B and C) Quantification of CellVue Far Red-labeled dead cell engulfment by hiDC and hiDC+cyt at day 9 after 2-hour incubation. HEF cultured without

and with cytokines (HEF+cyt) and CD141⁺CLEC9A⁺ cDC1 were included as controls (n=3-12, mean ± SD). **(D)** Time lapse microscopy of dead cell engulfment (red) by FACS purified hiDCs (arrowhead). Scale bar, 100 µm. **(E)** Dead cell engulfment by CD45⁺HLA-DR⁺CD226⁺ and CD45⁺HLA-DR⁺CD226⁻ hiDC and hiDC+cyt (n=6-7, mean ± SD). **(F)** Cytokine secretion of purified hiDC and hiDC+cyt at day 9 after overnight incubation with TLR agonists. HEFs cultured without and with cytokines, monocyte-derived DCs (moDC) and purified CD141⁺CLEC9A⁺XCR1⁺ cDC1 were included as controls (n=3-12, mean ± SD). **(G)** HEF, HEF+cyt, hiDC, hiDC+cyt, moDC and cDC1 were primed overnight with LPS, Poly I:C and R848, pulsed with CMV protein for 3 hours, washed and co-cultured with CD8⁺ T cells harvested from CMV⁺ donors. Antigen cross-presentation was quantified by measuring IFN-γ levels in the supernatant 24 h after co-culture (n=2-4, mean ± SD). * p<0.05; ** p<0.005; *** p<0.0005; **** p<0.00005.

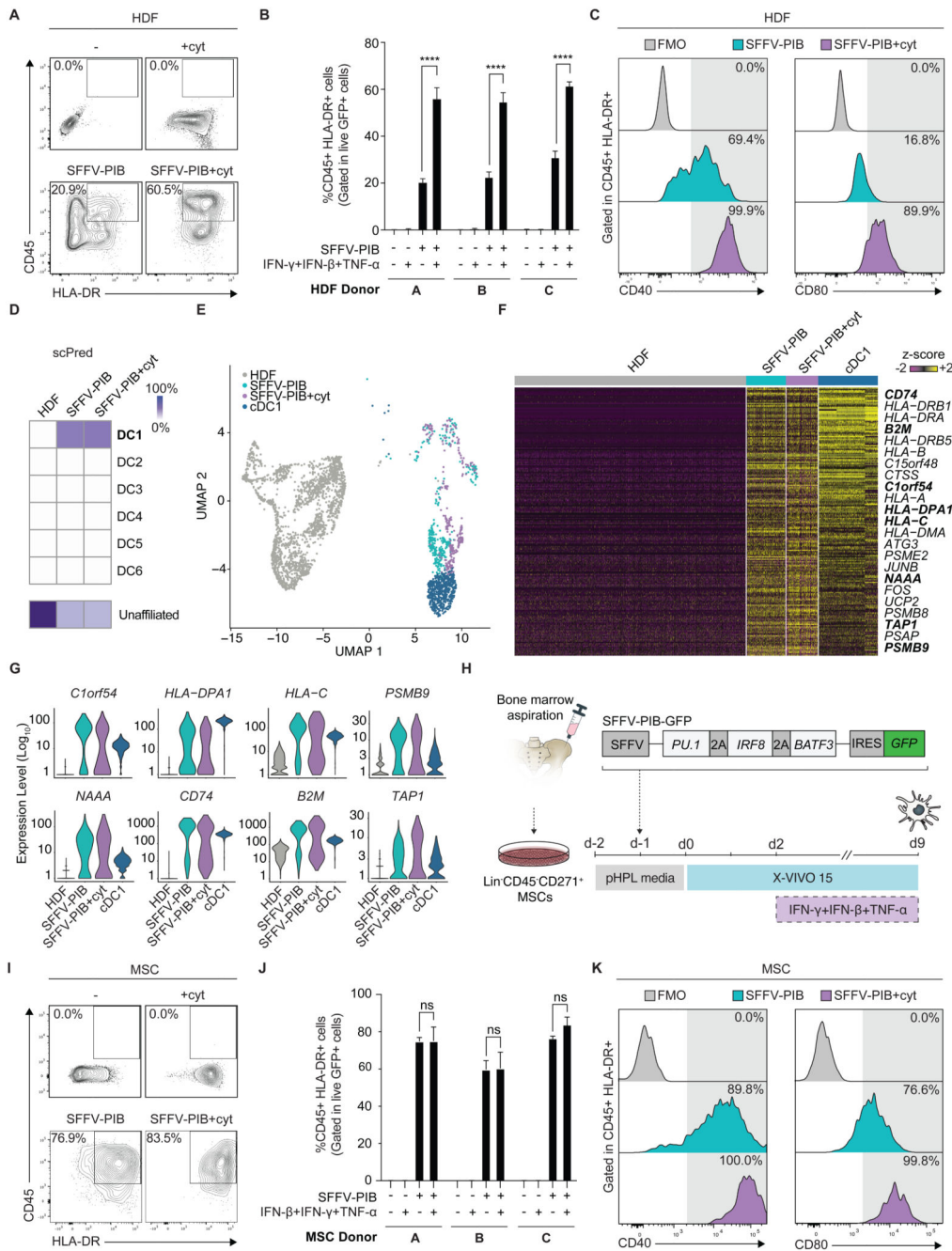


Fig. 5. Efficient cDC1 reprogramming of adult fibroblasts and mesenchymal stromal cells.

(A) Flow cytometry analysis and **(B)** quantification of hiDC (CD45⁺HLA-DR⁺) at day 9 generated from human dermal fibroblasts (HDF) in the absence (SFFV-PIB) or presence of IFN- γ , IFN- β and IFN- α (SFFV-PIB+cyt) from three independent donors. HDF cultured in the absence (-) or presence of cytokines (+cyt) were included as controls (n=3-12, mean \pm SD). **(C)** Expression of CD40 and CD80 in HDF-derived hiDC. **(D)** HDF-derived hiDC were FACS sorted and profiled by scRNA-seq. Heat map shows the percentage of single cells affiliated to DC1-6 subsets (7) by scPred (22). **(E)** t-SNE of single cell transcriptomes

showing HDFs, HDF-derived hiDCs and cDC1s. **(F)** Heat map showing relative expression of genes upregulated during cDC1 reprogramming of HDF and expressed in cDC1s. cDC1 and antigen presentation genes are highlighted in bold and shown in **(G)** as violin plots. Log values of gene counts are shown. **(H)** Strategy to derive hiDC from human Mesenchymal Stromal Cells (MSC) under xeno-free conditions. MSC were isolated from three healthy donors, FACS-purified ($\text{Lin}^- \text{CD45}^- \text{CD271}^+$), expanded in pHPL media, transduced and cultured in X-VIVO 15. **(I and J)** Quantification of MSC-derived hiDCs at day 9 generated with or without cytokines (n=3-7, mean \pm SD). **(K)** Flow cytometry analysis of CD40 and CD80 in MSC-derived hiDCs. ns - non significant; **** p<0.00005.

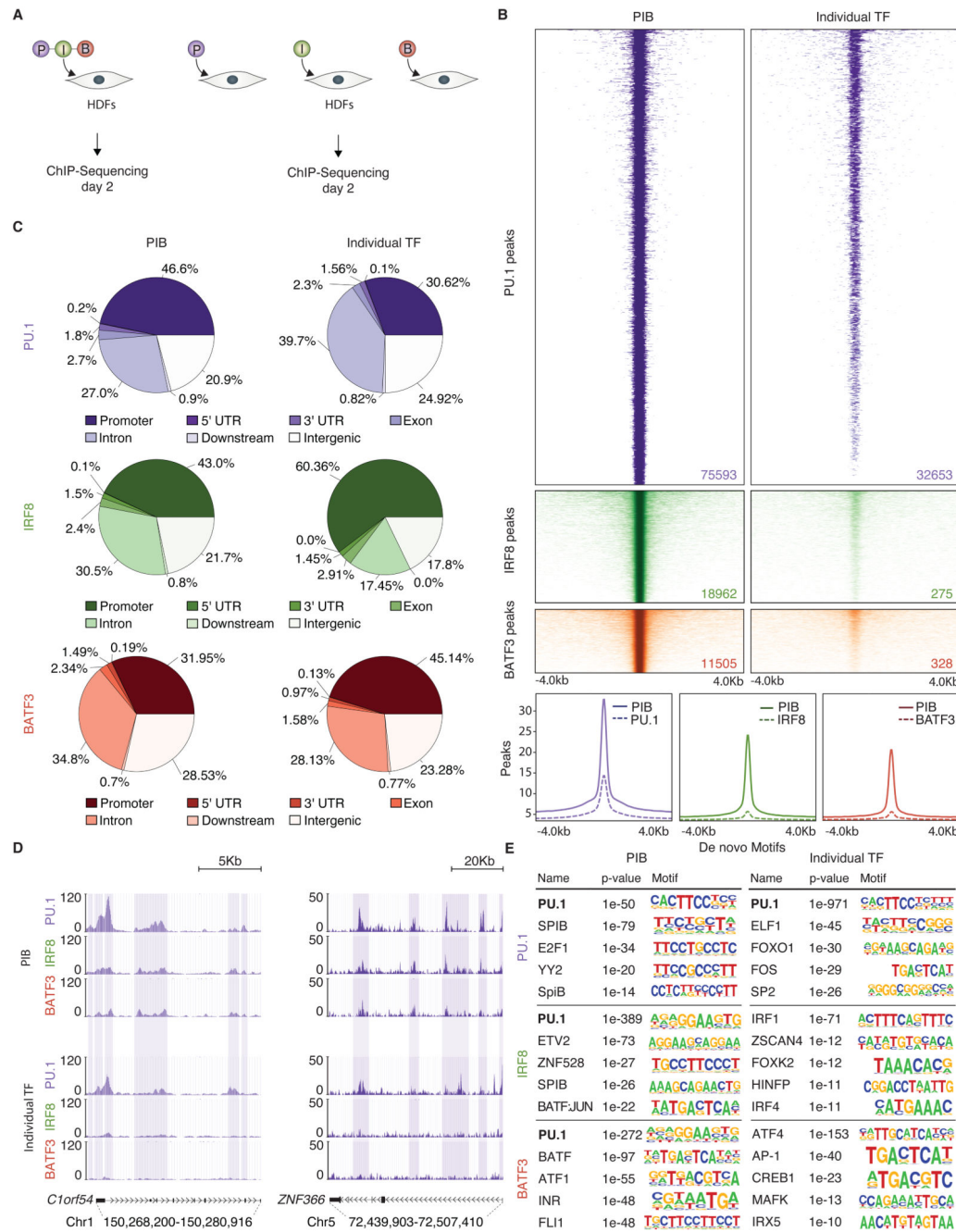


Fig. 6. PU.1 has dominant and independent chromatin targeting capacity, recruiting IRF8 and BATF3 to shared binding sites.

(A) Strategy to profile chromatin binding sites of PU.1, IRF8 and BATF3 (PIB) at early stages of reprogramming. HDFs were transduced with PIB (left) or individual factors (right) and analyzed by ChIP-seq after 48 hours. (B) Heatmaps showing genome-wide distribution of PU.1, IRF8 and BATF3 when expressed in combination (left) or individually (right). Signal is displayed within an 8 kb window centered on individual peaks. The number of peaks in each condition is shown. Average signal intensity of peaks is depicted (bottom). (C)

Pie charts showing genomic distribution of PU.1, IRF8 and BATF3 peaks when expressed together or individually. **(D)** PU.1, IRF8 and BATF3 occupancy profile at the *C1orf54* and *ZNF366* loci. Boxes highlight PU.1 peaks when expressed individually or combined with IRF8 and BATF3. **(E)** *De novo* motif prediction analysis for PIB or individual transcription factor target sites.

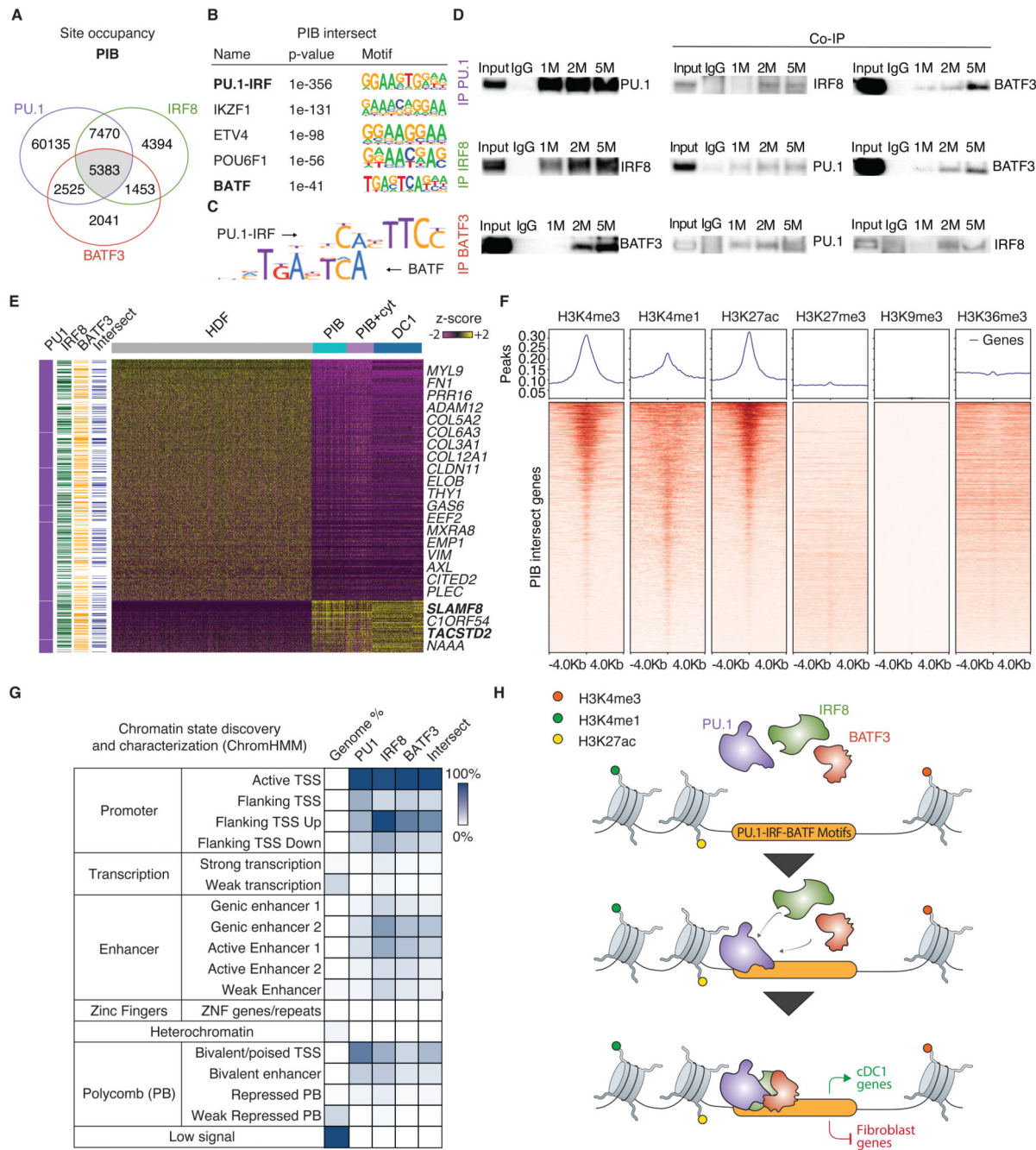


Fig. 7. PU.1, IRF8 and BATF3 cooperatively bind at fibroblast and cDC1 genes marked with open chromatin marks.

(A) Venn diagram shows genome-wide peak overlap between PU.1, IRF8 and BATF3 (PIB). (B) *De novo* motif prediction analysis for co-bound sites. (C) Motif comparison between enriched PU.1-IRF and BATF motifs. Jaccard similarity coefficient = 0.02. (D) Immunoblots showing immunoprecipitation (IP) for PU.1 (top), IRF8 (middle), and BATF3 (bottom) in HEK293T cells 24 hours after transfection with PIB (left). Co-immunoprecipitation (Co-IP) performed with 1, 2 and 5 million (M) cells after transfection with PIB (right).

Non-immunoprecipitated input (10%), and IgG isotype antibody were used as controls. **(E)** Heat map showing differentially expressed genes between HDFs and hiDC at day 9 that are bound by either PU.1, IRF8 and BATF3 or the three factors (intersect). **(F)** Heatmaps of normalized read coverages of chromatin marks in HDFs for co-bound sites. The signal is displayed within an 8 kb window and centered on transcription factor binding sites. Average signal intensity of histone marks at PIB intersection peaks is shown in the upper panel. **(G)** Heatmaps for chromatin state enrichment showing the percentage of genome occupancy for PU.1 (P), IRF8 (I) and BATF3 (B) when expressed together. Genome occupancy of co-bound sites (PIB intersect) is shown on the right. **(H)** Model for the mechanism of action of PIB to set in motion cDC1 reprogramming.